

Probing the Chemistry, Electronic Structure and Redox Energetics in Organometallic Pentavalent Uranium Complexes

Christopher R. Graves, Anthony E. Vaughn, Eric J. Schelter, Brian L. Scott, Joe D. Thompson, David E. Morris,* and Jaqueline L. Kiplinger*

Los Alamos National Laboratory, Los Alamos, New Mexico 87545

Received September 9, 2008

A series of organometallic pentavalent uranium complexes of the general formula $(C_5Me_5)_2U(=N-2,6-iPr_2-C_6H_3)(Y)$ (Y = monoanionic, non-halide ligand) have been prepared using a variety of routes. Utilizing the direct oxidation of $(C_5Me_5)_2U(=N-2,6-iPr_2-C_6H_3)(THF)$ (**2**) with the appropriate copper(I) salt yielded the triflate ($Y = OTf$ (OSO_2CF_3), **11**), thiolate ($Y = SPh$, **12**), and acetylide ($Y = C\equiv CPh$, **13**) complexes, while a salt metathesis route between the U^V -imido $(C_5Me_5)_2U(=N-2,6-iPr_2-C_6H_3)(I)$ (**10**) and various alkali salts gave the diphenylamide ($Y = NPh_2$, **14**), aryloxy ($Y = OPh$, **15**), alkyl ($Y = Me$, **16**), and aryl ($Y = Ph$, **17**) complexes. Paired with **13**, the isolation of **16** and **17** shows that U^V can support the full range of carbon anions (sp , sp^2 , and sp^3), and these are, to the best of our knowledge, the first examples of pentavalent uranium complexes with anionic carbon moieties other than carbocyclic (C_5R_5 , C_7H_7 , C_8H_8) ligands. Finally, both protonolysis and insertion pathways afforded the U^V -imido ketimide complex $(C_5Me_5)_2U(=N-2,6-iPr_2-C_6H_3)(N=CPh_2)$ (**18**). The complexes have been isolated in good yield and characterized using various combinations of 1H NMR spectroscopy, elemental analysis, mass spectrometry, single crystal X-ray diffraction, cyclic voltammetry, UV-visible-NIR absorption spectroscopy, and magnetic susceptibility measurements. All $(C_5Me_5)_2U(=N-Ar)(X)$ ($X = F, Cl, Br, I$) and $(C_5Me_5)_2U(=N-Ar)(Y)$ complexes exhibit U^{VI}/U^V and U^V/U^{IV} redox couples by voltammetry. The potential separation between these couples remains essentially constant at ~ 1.50 V, but both processes shift in tandem in potential by ~ 700 mV across the series of X/Y ligands. No significant differences between μ_{eff} values or temperature dependencies in the magnetic susceptibility were observed for these complexes regardless of the identity of the ancillary X/Y ligand. However, an excellent linear correlation was observed between the chemical shift values of C_5Me_5 ligand protons in the 1H NMR spectra and the oxidation potentials of $(C_5Me_5)_2U(=N-2,6-iPr_2-C_6H_3)(X/Y)$, suggesting that there is a common origin, overall σ/π -donation from the ancillary X/Y ligand to the metal, contributing to both observables. Combined, these data confer the following trend in increasing σ/π -donating ability of the X/Y ligand to the U^V metal center: $OTf < I < Br < Cl < SPh < C\equiv CPh < F < [OPh \sim Me \sim Ph] \ll NPh_2 < N=CPh_2$. These $(C_5Me_5)_2U(=N-2,6-iPr_2-C_6H_3)(X/Y)$ complexes also show distinct hallmarks of a covalent bonding interaction between the metal and the imide ligand that is modulated to varying degrees by the interaction between the X/Y ancillary ligand and the U^V metal center. These signatures of covalency include stabilization of multiple metal oxidation states [U^{VI} , U^V , and U^{IV}] and enhanced intensities in the intraconfiguration (f-f) transitions. Of particular note in this regard is the more than 20-fold enhancement in the f-f intensities observed for $Y = C\equiv CPh$ and $N=CPh_2$, which is a clear reflection of the covalent metal-ligand bonding interactions sustained by the acetylide and ketimide ligands in these pentavalent systems.

Introduction

Complexes of the early actinides (Th–Pu) have gained considerable prominence in organometallic chemistry as they have been shown to undergo chemistries not observed with their transition- or lanthanide metal counterparts.^{1–9} Further, while bonding in f-element complexes has historically been

considered to be ionic, the issue of covalency remains a subject of debate in the area of actinide science,^{10–14} and studies aimed at elucidating key bonding interactions with 5f-orbitals continue to garner attention. Towards this end, our interests have focused on the role that metal oxidation state plays in the structure, reactivity, and spectral properties

* To whom correspondence should be addressed. E-mail: kiplinger@lanl.gov.

(1) For a recent review of the chemistry concerning U^{III} as a reducing agent, see: (a) Evans, W. J.; Kozimor, S. A. *Coord. Chem. Rev.* **2006**, *250*, 911–935.

of organouranium complexes. In recent years, tetravalent and hexavalent complexes have dominated the landscape of uranium chemistry,^{15,16} with the corresponding pentavalent systems remaining rare. This is presumably a consequence of their instability towards redistribution,^{17,18} and most of our current knowledge of the physicochemical properties of uranium in this oxidation state come from classical coordination complexes of the halides, (e.g., UX_5 where X = halide).^{19,20}

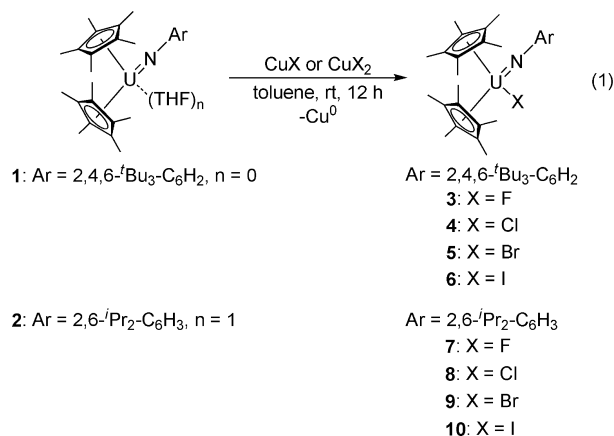
From a heuristic perspective, the U^V oxidation state with its simple $5f^1$ valence electronic configuration remains a highly attractive target. While more structurally elaborate uranium(V) systems have been noted in the literature, specifically those containing metal–nitrogen and -oxygen bonds,^{13,21} systems containing U–carbon bonds are comparatively less common.^{15,22} Generally speaking, the synthetic routes available for accessing pentavalent systems have been limited, relying on either the one-electron oxidation of U^{IV} complexes with silver^{22a,23} or thallium²⁴ salts to give the corresponding U^V species, or by reacting trivalent

uranium complexes with powerful two-electron oxidants such as azides or *N*-oxides to give the corresponding U^V -imido or -oxo complexes, respectively.^{21c,25–28} While successful, these routes utilize reagents that can be difficult to handle and control,²⁹ and are also synthetically limited in scope and cannot be easily fine-tuned.

We recently reported^{30–32} a general and versatile Cu(I)-based oxidation procedure that enables easy access to pentavalent organometallic uranium complexes of the type $(C_5Me_5)_2U(=N-Ar)(X)$ (where X = halide) from the corresponding U^{IV} -imido systems ($(C_5Me_5)_2U(=N-2,4,6-tBu_3C_6H_2)$ (**1**);³³ $(C_5Me_5)_2U(=N-2,6-Pr_2-C_6H_3)$ (**2**)²⁵) (eq 1). While the one-electron oxidations utilizing silver salts have produced cationic uranium complexes, this Cu-based oxidative functionalization results in neutral U^V species which feature a bent-metallocene framework with the imido and halide ligands contained within the metallocene wedge.

Applicable for the synthesis of the full suite of halides (X = F, Cl, Br, I), this protocol allowed for a systematic study of the electronic structure and bonding in these pentavalent uranium halides—a study which suggested that only minor differences existed between the structures as the halide ligand was varied. As such, our search has been broadened to include the synthesis of non-halide U^V -imido complexes, $(C_5Me_5)_2U(=N-Ar)(Y)$ (where Y = non-halide monoanionic

- (2) While transition metal complexes follow the 18-electron rule, no such rule exists for the actinides. For pertinent examples, see: (a) Reynolds, L. T.; Wilkinson, G. J. *Inorg. Nucl. Chem.* **1956**, *2*, 246–253. (b) Fischer, E. O.; Hristidu, Y. Z. *Naturforsch.* **1962**, *173*, 275–276. (c) Streitwieser, A., Jr.; Mueller-Westerhoff, U. *J. Am. Chem. Soc.* **1968**, *90*, 7364. (d) Avdeef, A.; Raymond, K. N.; Hodgson, K. O.; Zalkin, A. *Inorg. Chem.* **1972**, *11*, 1083–1088. (e) Maier, R.; Kanellakopulos, B.; Apostolidis, C.; Meyer, D.; Rebizant, J. *J. Alloys Compd.* **1993**, *190*, 269–271.
- (3) Schelter, E. J.; Yang, P.; Scott, B. L.; Da Re, R. E.; Jantunen, K. C.; Martin, R. L.; Hay, P. J.; Morris, D. E.; Kiplinger, J. L. *J. Am. Chem. Soc.* **2007**, *129*, 5139–5152.
- (4) Schelter, E. J.; Yang, P.; Scott, B. L.; Thompson, J. D.; Martin, R. L.; Hay, P. J.; Morris, D. E.; Kiplinger, J. L. *Inorg. Chem.* **2007**, *46*, 7477–7488.
- (5) Schelter, E. J.; Morris, D. E.; Scott, B. L.; Kiplinger, J. L. *Chem. Commun.* **2007**, 1029–1031.
- (6) Kiplinger, J. L.; Pool, J. A.; Schelter, E. J.; Thompson, J. D.; Scott, B. L.; Morris, D. E. *Angew. Chem., Int. Ed.* **2006**, *45*, 2036–2041.
- (7) Jantunen, K. C.; Scott, B. L.; Kiplinger, J. L. *J. Alloys Compd.* **2007**, *444–445*, 363–368.
- (8) Pool, J. A.; Scott, B. L.; Kiplinger, J. L. *Chem. Commun.* **2005**, 2591–2593.
- (9) Pool, J. A.; Scott, B. L.; Kiplinger, J. L. *J. Am. Chem. Soc.* **2005**, *127*, 1338–1339.
- (10) Burns, C. J.; Bursten, B. E. *Comments Inorg. Chem.* **1989**, *9*, 61–93.
- (11) Diaconescu, P. L.; Arnold, P. L.; Baker, T. A.; Mendiola, D. J.; Cummins, C. C. *J. Am. Chem. Soc.* **2000**, *122*, 6108–6109.
- (12) Mazzanti, M.; Wietzke, R.; Pecaut, J.; Latour, J.-M.; Maldivi, P.; Remy, M. *Inorg. Chem.* **2002**, *41*, 2389–2399.
- (13) Meyer, K.; Mendiola, D. J.; Baker, T. A.; Davis, W. M.; Cummins, C. C. *Angew. Chem., Int. Ed.* **2000**, *39*, 3063–3066.
- (14) Raymond, K. N.; Eigenbrot, C. W., Jr. *Acc. Chem. Res.* **1980**, *13*, 276–283.
- (15) Burns, C. J.; Eisen, M. S. *Organoactinide Chemistry: Synthesis and Characterization*. In *The Chemistry of the Actinide and Transactinide Elements*, 3rd ed.; Morss, L. R., Edelstein, N. M., Fuger, J., Eds.; Springer: The Netherlands, 2006; Vol. 5, pp 2799–2910, and references therein.
- (16) Ephritikhine, M. *Dalton Trans.* **2006**, 2501–2516.
- (17) For a review on the synthesis, stability and properties of pentavalent uranium, see: (a) Selbin, J.; Ortego, J. D. *Chem. Rev.* **1969**, *69*, 657–621.
- (18) Bagnall, K. W. *Comprehensive Coordination Chemistry*; Wilkinson, G., Gillard, R. D., Mc Cleverty, J. A., Eds.; Pergamon: Oxford, 1987; Vol. 3, p 1129.
- (19) For a detailed list of various U^V halide complexes, see: Grenthe I.; Drozdzyński, J.; Fujino, T.; Buck, E. C.; Albrecht-Schmitt, T. E.; Wolf, S. F. *Uranium*. In *The Chemistry of the Actinide and Transactinide Elements*, 3rd ed.; Morss, L. R., Edelstein, N. M., Fuger, J., Eds.; Springer: The Netherlands, 2006; Vol. 1, pp 501–529.
- (20) Ryan, J. L. *J. Inorg. Nucl. Chem.* **1971**, *33*, 153–177.
- (21) For representative examples of U^V -amide and -alkoxide/aryloxide complexes, see: (a) Zalkin, A.; Brennan, J. G.; Andersen, R. A. *Acta Crystallogr.* **1988**, *C44*, 1553–1554. (b) Roussel, P.; Hitchcock, P. B.; Tinker, N. D.; Scott, P. *Inorg. Chem.* **1997**, *36*, 5716–5721. (c) Castro-Rodriguez, I.; Olsen, K.; Meyer, K. *J. Am. Chem. Soc.* **2003**, *125*, 4565–4571. (d) Salmon, P.; Thuery, P.; Ephritikhine, M. *Polyhedron* **2007**, *26*, 631–636. (e) Hayton, T. W.; Wu, G. *J. Am. Chem. Soc.* **2008**, *130*, 2005–2014.
- (22) For examples of organometallic pentavalent uranium complexes, see: (a) Boisson, C.; Berthet, J.-C.; Lance, M.; Nierlich, M.; Vigner, J.; Ephritikhine, M. *J. Chem. Soc., Chem. Commun.* **1995**, 543–544. (b) Gourier, D.; Caurant, D.; Berthet, J. C.; Boisson, C.; Ephritikhine, M. *Inorg. Chem.* **1997**, *36*, 5931–5936. (c) Ephritikhine, M.; Berthet, J. C.; Boisson, C.; Lance, M.; Nierlich, M. *J. Alloys Compd.* **1998**, *271–273*, 144–149. (d) Arliguie, T.; Rourmigue, M.; Ephritikhine, M. *Organometallics* **2000**, *19*, 109–111; also see reference 25.
- (23) Boisson, C.; Berthet, J.-C.; Lance, M.; Vigner, J.; Nierlich, M.; Ephritikhine, M. *J. Chem. Soc., Dalton Trans.* **1996**, 947–953.
- (24) Berthet, J. C.; Ephritikhine, M. *J. Chem. Soc., Chem. Commun.* **1993**, 1566–1567.
- (25) Arney, D. S. J.; Burns, C. J. *J. Am. Chem. Soc.* **1993**, *115*, 9840–9841.
- (26) Brennan, J. G.; Andersen, R. A. *J. Am. Chem. Soc.* **1985**, *107*, 514–516.
- (27) Castro-Rodriguez, I.; Nakai, H.; Meyer, K. *Angew. Chem., Int. Ed.* **2006**, *45*, 2389–2392.
- (28) Roussel, P.; Boaretto, R.; Kingsley, A. J.; Alcock, N. W.; Scott, P. *J. Chem. Soc., Dalton Trans.* **2002**, 1423–1428.
- (29) Although silver salts are among the most widely utilized oxidants for metal complexes, their behavior can be difficult to predict and control. For an excellent review on chemical oxidants for organometallic systems, see: (a) Connelly, N. G.; Geiger, W. E. *Chem. Rev.* **1996**, *96*, 877–910.
- (30) This protocol has also been successfully extended to the oxidative functionalization of U^{III} organometallics to their U^{IV} equivalent, see: Graves, C. R.; Schelter, E. J.; Cantat, T.; Scott, B. L.; Kiplinger, J. L. *Organometallics* **2008**, *27*, 5371–5378.
- (31) Graves, C. R.; Scott, B. L.; Morris, D. E.; Kiplinger, J. L. *J. Am. Chem. Soc.* **2007**, *129*, 11914–11915.
- (32) Graves, C. R.; Yang, P.; Kozimor, S. A.; Vaughn, A. E.; Clark, D. L.; Conradson, S. D.; Schelter, E. J.; Scott, B. L.; Thompson, J. D.; Hay, P. J.; Morris, D. E.; Kiplinger, J. L. *J. Am. Chem. Soc.* **2008**, *130*, 5272–5285.
- (33) Arney, D. S. J.; Burns, C. J. *J. Am. Chem. Soc.* **1995**, *117*, 9448–9460.

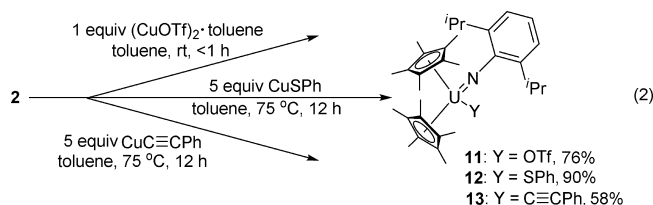


ligand) to investigate larger variations in the bonding environment around the uranium metal. Herein, we report our progress in the synthesis of substituted U^V-imido complexes using various routes: (1) Direct oxidation of U^{IV}-imido complexes with copper(I) salts; (2) Salt metathesis with U^V-imido halides; (3) Protonolysis and insertion of an U^V-imido alkyl or aryl complex with H–N=CPh₂ or N≡CPh, respectively, to form a U^V-imido ketimide complex. Further, we report and compare the crystallographic, electrochemical, spectroscopic, and magnetic characterization of the pentavalent uranium (C₅Me₅)₂U(=N–Ar)(Y) series (Y = OTf, SPh, C≡CPh, NPh₂, OPh, Me, Ph, N=CPh₂) to further interrogate the molecular, electronic, and magnetic structures of this new class of uranium complexes.

Results and Discussion

Synthesis and Structural Characterization. I. Direct Oxidation. The direct oxidation of complex **2** with functionalized copper(I) salts was examined as a primary route for the synthesis of (C₅Me₅)₂U(=N-2,6-*i*Pr₂-C₆H₃)(Y) complexes with extended ligand sets (Y ≠ halide). A logical extension of the halide chemistry, reaction of **2** with 1 equiv of the (CuOTf)₂·toluene adduct (OTf = OSO₂CF₃) afforded the U^V-imido triflate derivative, (C₅Me₅)₂U(=N-2,6-*i*Pr₂-C₆H₃)(OTf) (**11**), in good isolated yield (eq 2).³¹ Oxidations using the copper halides were optimized to occur over 12 h with an excess of the oxidant (5 equiv); however, use of excess (CuOTf)₂·toluene or extended reaction times lead to decomposition of the triflate product. Conversely, (C₅Me₅)₂U(=N-2,6-*i*Pr₂-C₆H₃)(SPh) (**12**)³¹ and (C₅Me₅)₂U(=N-2,6-*i*Pr₂-C₆H₃)(C≡CPh) (**13**)³⁴ could only be prepared by reacting **2** with excess oxidant (CuSPh or CuC≡CPh, 5 equiv) at 75 °C over 12 h. Following workup, complexes **11**–**13** were reproducibly isolated as analytically pure solids and were characterized by a combination of ¹H NMR, electrochemistry, UV-visible near-IR spectroscopy, elemental and mass spectrometric analyses, and magnetic susceptibility.

The identities of compounds **11** and **12** were confirmed by single-crystal X-ray crystallography.³¹ Like their halide counterparts, these bent-metallocene complexes contain the imido and Y ligands within the metallocene wedge. A list



of selected geometric parameters can be found in Table 1. Both **11** and **12** have nearly linear U=N–C_{Ar} angles (168.3(5)° and 171.6(3)°, respectively) and short U=N_{imido} bond distances (1.9575(5) Å and 1.976(4) Å, respectively), which compare well with the corresponding metrical parameters observed for the structurally characterized U^V-imido halides (**3**, **5**, **8**–**10**)³² and other high-valent uranium (U^{IV}, U^V, U^{VI}) imido compounds.³⁵ To the best of our knowledge, complex **11** is the first structurally characterized pentavalent uranium species incorporating a triflate group. At 2.378(4) Å, the U–OTf bond length observed in **11** is similar to those reported for other structurally characterized uranium triflate complexes. For example, (C₅Me₅)₂U[η²-(N,N′)-CH₃-N=N=CPh₂](OTf) has a U–OTf bond distance of 2.395(14) Å,³⁶ while the U^{IV} bis(triflate) complexes (C₅Me₅)₂U(OTf)₂·OH₂ and (C₅H₅)₂U(OTf)₂(pyridine)₂ have U–OTf bond lengths of 2.36(1) Å and 2.40(1) Å³⁷ and 2.395(4) Å and 2.385(4) Å,³⁸ respectively. For comparison with **12**, one other pentavalent organouranium complex with a U–S bond has been reported: [Na(18-crown-6)(THF)][(η⁸-C₈H₈)U-(C₄H₄S₄)₂], with U–S bond lengths in the range 2.687(2)–2.700(2) Å.^{39,40} Not surprisingly, the U–S distance of 2.7230(13) Å found for neutral **12** is slightly longer than the range observed for the U^V cationic system, but it is in agreement with U–S bond distances observed for complexes of uranium in other oxidation states.⁴¹

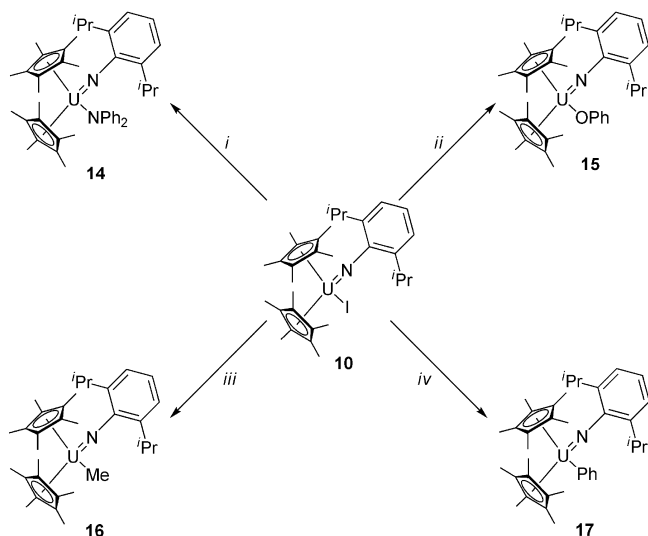
II. Salt Metathesis. An alternative route for the generation of substituted U^V-imido complexes is salt metathesis from

- (35) For other examples of imido complexes featuring short U=N bond distances (Å) and nearly linear U=N–C imido angles (deg), see: (a) Brennan, J. G.; Andersen, R. A. *J. Am. Chem. Soc.* **1985**, *107*, 514–516. (b) Stewart, J. L. Tris[bis(trimethylsilyl)amido]uranium: Compounds with Tri-, Tetra-, and Pentavalent Uranium. Ph. D. Dissertation, University of California, Berkeley, CA, 1988. (c) Arney, D. S. J.; Burns, C. J.; Smith, D. C. *J. Am. Chem. Soc.* **1992**, *114*, 10068–10069. (d) Roussel, P.; Boaretto, R.; Kingsley, A. J.; Alcock, N. W.; Scott, P. *J. Chem. Soc., Dalton Trans.* **2002**, 1423–1428. (e) Hayton, T. W.; Boncella, J. M.; Scott, B. L.; Palmer, P. D.; Batista, E. R.; Hay, P. J. *Science* **2005**, *310*, 1941–1943. (f) Zi, G.; Jia, L.; Werkema, E. L.; Walter, M. D.; Gottfriedsen, J. P.; Andersen, R. A. *Organometallics* **2005**, *24*, 4251–4264. (g) Hayton, T. W.; Boncella, J. M.; Scott, B. L.; Batista, E. R.; Hay, P. J. *J. Am. Chem. Soc.* **2006**, *128*, 10549–10559. (h) Spencer, L. P.; Yang, P.; Scott, B. L.; Batista, E. R.; Boncella, J. M. *J. Am. Chem. Soc.* **2008**, *130*, 2930–2931; also see references 21a, c, 25, 31, 32, 44d. (36) Kiplinger, J. L.; John, K. D.; Morris, D. E.; Scott, B. L.; Burns, C. J. *Organometallics* **2002**, *21*, 4306–4308. (37) Berthet, J. C.; Lance, M.; Nierlich, M.; Ephritikhine, M. *Chem. Commun.* **1998**, 1373–1374. (38) Berthet, J. C.; Nierlich, M.; Ephritikhine, M. *Eur. J. Inorg. Chem.* **2002**, 850–858. (39) Arliguie, T.; Fourmigue, M.; Ephritikhine, M. *Organometallics* **2000**, *19*, 109–111. (40) Belkhir, L.; Arliguie, T.; Thuery, P.; Fourmigue, M.; Boucekkine, A.; Ephritikhine, M. *Organometallics* **2006**, *25*, 2782–2795.

(34) Graves, C. R.; Scott, B. L.; Morris, D. E.; Kiplinger, J. L. *Organometallics* **2008**, *27*, 3335–3337.

Table 1. Selected Metrical Parameters for the $(C_5Me_5)_2U(=N-2,6-iPr_2-C_6H_3)(X/Y)$ Complexes **8–12, 14, 18**

	$C_5Me_5(cent)-U$		imido parameters			X/Y ligand parameters		N–U–X/Y (deg)
	(Å)	$C_5Me_5(cent)-U-$ $C_5Me_5(cent)$ (deg)	U=N (Å)	N–C (Å)	U=N–C (deg)			
8 X = Cl	2.505, 2.453	134.87	1.963(4)	1.404(7)	169.6(4)	U–Cl (Å) 2.6209(15)	N–U–Cl 105.79(13)	
9 X = Br	2.523, 2.452	137.98	1.969(7)	1.40(2)	172.2(9)	U–Br (Å) 2.789(3)	N–U–Br 105.3(2)	
10 X = I	2.454, 2.459	134.07	1.974(7)	1.406(10)	170.7(6)	U–I (Å) 3.0385(7)	N–U–I 106.6(2)	
11 Y = OTf	2.435, 2.440	135.92	1.9575(5)	1.416(8)	168.3(5)	U–O (Å) 2.378	U–O–S (deg) 160.4(3)	N–U–O 109.16(19)
12 Y = SPh	2.466, 2.457	136.24	1.976(4)	1.398(6)	171.6(3)	U–S (Å) 2.7230(13)	U–S–C(deg) 131.08(17)	N–U–S 103.35(12)
14 Y = NPh ₂	2.511, 2.530	125.01	1.984(4)	1.399(6)	174.0(3)	U–N (Å) 2.322(4)	N–U–N 93.73(15)	
18 Y = N=CPh ₂	2.493, 2.484	138.32	2.012(4)	1.391(7)	174.6(4)	U–N (Å) 2.199(4)	U–N–C (deg) 177.8(4)	N–U–N 111.99(17)

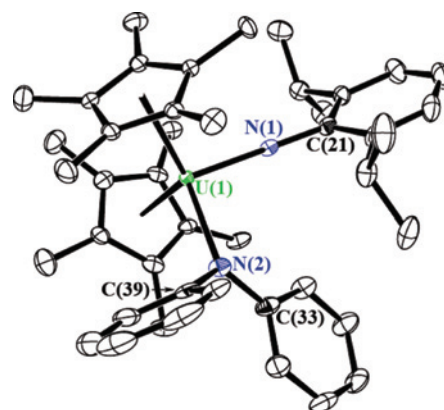
Scheme 1. Salt Metathesis Route to Substituted U^V -Imido Organometallic Complexes^a

^a *i*: 1.2 equiv KNPh₂, toluene, 25 °C, 12 h, 80%; *ii*: 1.2 equiv KOPh, toluene, 75 °C, 12 h, 75%; *iii*: 1.5 equiv Me₂Mg, 1,4-dioxane, toluene, 25 °C, 12 h, 70%; *iv*: 2.0 equiv Ph₂Mg(THF)₂, 1,4-dioxane, toluene, 25 °C, 12 h, 80%.

the imido iodide $(C_5Me_5)_2U(=N-2,6-iPr_2-C_6H_3)(I)$ (**10**)⁴² using alkali metal reagents. This pathway is particularly attractive for experimental conditions where the copper(I) reagent required for the direct oxidation pathway outlined above is unavailable or unstable; use of salt metathesis expands the breadth of the U^V -imido chemistry and available structural types. As illustrated in Scheme 1, $(C_5Me_5)_2U(=N-2,6-iPr_2-C_6H_3)(NPh_2)$ (**14**) was prepared by the reaction between **10** and KNPh₂. While this reaction occurred at room temperature over 12 h, the corresponding synthesis for $(C_5Me_5)_2U(=N-2,6-iPr_2-C_6H_3)(OPh)$ (**15**) required elevated temperatures (75 °C) to occur in an equivalent timeframe.

(41) U–S distances in the range of ~2.6–2.8 Å have been reported for trivalent uranium complexes. For examples, see: (a) Clark, D. L.; Miller, M. M.; Watkin, J. G. *Inorg. Chem.* **1993**, *32*, 772–774. (b) Leverd, P. C.; Ephritikhine, M.; Lance, M.; Vigner, J.; Nierlich, M. *J. Organomet. Chem.* **1996**, *507*, 229–237. (c) Lescop, C.; Arliguie, T.; Lance, M.; Nierlich, M.; Ephritikhine, M. *J. Organomet. Chem.* **1999**, *580*, 137–144. (d) Diaconescu, P. L.; Arnold, P. L.; Baker, T. A.; Mindiola, D. J.; Cummins, C. C. *J. Am. Chem. Soc.* **2000**, *122*, 6108–6109. (e) Arliguie, T.; Lescop, C.; Ventelon, L.; Leverd, P. C.; Thuery, P.; Nierlich, M.; Ephritikhine, M. *Organometallics* **2001**, *20*, 3698–3703.

(42) Experiments performed on an NMR scale indicated that the corresponding Cl (**8**), Br (**9**), and OTf (**11**) complexes also react cleanly and can serve as starting materials using this salt metathesis route.

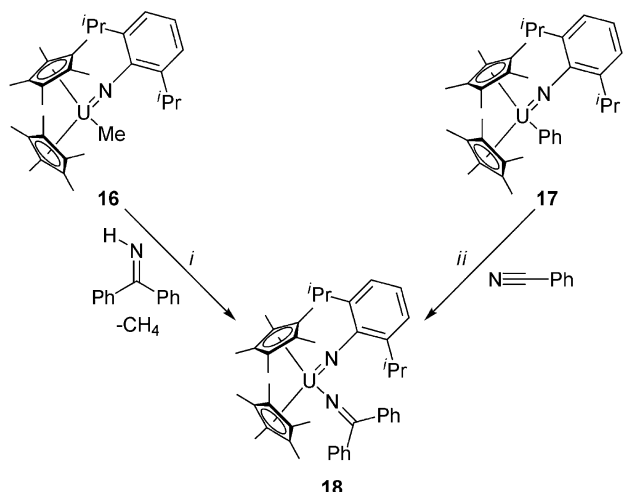
**Figure 1.** Molecular structure of complex **14** with thermal ellipsoids projected at the 50% probability level.

Both **14** and **15** were obtained in good isolated yields.

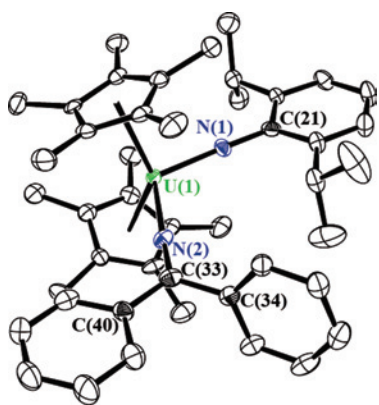
The molecular structure of **14** was confirmed by single-crystal X-ray diffraction (Figure 1);⁴³ the metrical parameters of **14** agree well with those observed for complexes **11** and **12**. Further, the U–N_{imido} distance and U=N–C_{Ar} angle of 1.984(4) Å and 174.0(3)° for **14** are in agreement with those found for the other U^V -imido complexes.³⁵ At 2.322(4) Å, the U(1)–N(1) bond in **14** compares well with the geometric parameters obtained for other neutral $((Me_3Si-N=)U-[N(SiMe_3)_2]_3)$, U–N_{amide} = 2.295(10) Å,^{21a} anionic $([U(dbabh)_6]^-)$ (Hdbabh = 2,3:5,6-dibenzo-7-azabicyclo[2.2.1]hepta-2,5-diene), U–N_{amide} = 2.230(11)–2.267(13) Å¹³ and cationic $([(C_5Me_5)U(NMe_2)_3(THF)]^+)$, U–N_{amide} = 2.25(2)–2.35(5) Å; $[(C_5Me_5)U(NEt_2)_2]^+$, U–N_{amide} = 2.162(9), 2.167(9) Å^{22a} uranium(V) complexes containing an U–N_{amide} linkage.⁴⁴

Complex **10** also served as a useful platform for the synthesis of both U^V -imido alkyl and aryl compounds—reaction between **10** and either Me₂Mg or Ph₂Mg(THF)₂ afforded the alkyl $(C_5Me_5)_2U(=N-2,6-iPr_2-C_6H_3)(Me)$ (**16**) and aryl $(C_5Me_5)_2U(=N-2,6-iPr_2-C_6H_3)(Ph)$ (**17**) complexes, respectively, in good isolated yield (Scheme 1). Paired with **13**, the isolation of **16** and **17** shows that U^V can support the full range of carbon anions (sp, sp², and sp³), and these are, to the best of our knowledge, the first examples of pentava-

(43) While publication quality data for the structure of **15** were not obtained, collected data showing connectivity consistent with the molecular framework of $(C_5Me_5)_2U(=N-2,6-iPr_2-C_6H_3)(OPh)$ were obtained.

Scheme 2. Synthesis of $(C_5Me_5)_2U(=N-2,6-iPr_2-C_6H_3)(N=CPh_2)$ (**18**) Using Protonolysis Routes from U^V -Imido Alkyl and Aryl Complexes^a

^a *i*: 1.2 equiv benzophenone imine, toluene, 75 °C, 12 h, 86%; *ii*: 1.2 equiv benzonitrile, toluene, 12 h, 91%.

**Figure 2.** Molecular structure of complex **18** with thermal ellipsoids projected at the 50% probability level.

lent uranium complexes with anionic carbon moieties other than carbocyclic (C_5R_5 , C_7H_7 , C_8H_8) ligands.^{15,22}

III. Protonolysis and Insertion. $(C_5Me_5)_2U(=N-2,6-iPr_2-C_6H_3)(Me)$ (**16**) and $(C_5Me_5)_2U(=N-2,6-iPr_2-C_6H_3)(Ph)$ (**17**) served as useful starting materials for the synthesis of the U^V -imido ketimide complex $(C_5Me_5)_2U(=N-2,6-iPr_2-C_6H_3)(N=CPh_2)$ (**18**) (Scheme 2). Complex **16**, prepared in situ, was heated at 75 °C in the presence of excess benzophenone imine to afford **18** in good isolated yield (86%) through protonolysis and concomitant loss of methane. Alternatively, insertion of benzonitrile into the $U-C_{aryl}$ bond of in situ formed **17** gave the identical product **18** in 91% yield. These pathways not only extend the scope of this U^V -imido chemistry but also confirm the existence of both **16** and **17**, which were not structurally characterized.

Single crystals of **18** suitable for X-ray diffraction studies were obtained by slow evaporation of a concentrated hexamethyldisiloxane solution at room temperature. Complex **18** (Figure 2) represents the first uranium-ketimide complex with the metal in a pentavalent oxidation state. As with complexes **11–15**, **18** has a nearly linear $U=N-C_{Ar}$ angle ($C(21)-N(1)-U(1) = 174.6(4)^\circ$) and a short $U=N_{imido}$ bond distance ($U(1)-N(1) = 2.012(4)$ Å). The $U-N_{ketimide}$ bond

length ($U(1)-N(2) = 2.199(4)$ Å) and nearly linear $U-N=C$ bond angle ($U(1)-N(2)-C(33) = 178.2(5)^\circ$) found in **18** are comparable to those found for other structurally characterized uranium ketimide complexes ($U-N_{ketimide} = 2.179(6)-2.220(3)$ Å).^{4,36,45–48}

Magnetic Susceptibility. The magnetic response of the $(C_5Me_5)_2U(=N-2,6-iPr_2-C_6H_3)(Y)$ complexes **11–15** and **18** was measured between 2 and 350 K to evaluate changes in the magnetic properties based on varying the auxiliary ligand (Y). With μ_{eff} (μ_B/U) values of 2.65 (**11**), 2.48 (**12**), 2.22 (**13**), 2.27 (**14**), 2.38 (**15**), and 2.03 (**18**) (determined from fitting the linear portion of the $1/\chi$ vs T data) the U^V -imido complexes exhibit magnetic susceptibilities similar to those observed for their U^V -imido halide counterparts³² and other reported pentavalent uranium complexes.^{17,21c,49–53} No significant differences in μ_{eff} values or temperature dependencies were observed for these complexes regardless of the identity of Y. Plots of both the χT product versus T and constant temperature magnetization (M versus H) at 2 K are provided as Supporting Information.

¹H NMR Spectroscopy. The ¹H NMR spectra of the U^V complexes **11–13** and **15–18**⁵⁴ are similar to those found for the U^V -imido halides—they exhibit a signal corresponding to the C_5Me_5 ligand protons and an inequivalency of the *ortho* *i*Pr groups not seen for the U^{IV} imido starting material.²⁵ As has been observed for other paramagnetic uranium systems,⁵⁵ there is a dependence on the chemical shift for like protons (i.e. the C_5Me_5 resonances) and the identity of the donating ligand (X or Y) in the paramagnetic $(C_5Me_5)_2U(=N-2,6-iPr_2-C_6H_3)(X/Y)$ framework (Table 2). While the exact reasons

- (44) The $U-N_{amide}$ bond length for **14** also compares well to $U-N_{amide}$ bond lengths for tri-, tetra- and hexavalent uranium amide complexes. For examples, see: (a) $U[N(SiMe_3)_2]_3$, $U-N_{amide} = 2.320(4)$ Å Stewart, J. L.; Andersen, R. A. *Polyhedron* **1998**, *17*, 953–958. (b) $(C_5Me_5)_2U[N(SiMe_3)_2]$, $U-N_{amide} = 2.352(2)$ Å Evans, W. J.; Nyce, G. W.; Forrestal, K. J.; Ziller, J. W. *Organometallics* **2002**, *21*, 1050–1055. (c) $(C_5Me_5)_2U[NH(2,6-Me_2-C_6H_3)]_2$, $U-U-N_{amide} = 2.276(6)$ Å Straub, T.; Frank, W.; Reis, G.; Eisen, M. S. *J. Chem. Soc., Dalton Trans.* **1996**, 2541–2546. (d) $[N(SiMe_3)_2]_3U(=N-SiMe_3)(F)$, $U-N_{amide} = 2.217(17) - 2.252(17)$ Å; $[N(SiMe_3)_2]_3U(=N-C_6H_5)(F)$, $U-N_{amide} = 2.206(7) - 2.226(6)$ Å Burns, C. J.; Smith, W. H.; Huffman, J. C.; Sattelberger, A. P. *J. Am. Chem. Soc.* **1990**, *112*, 3237–3238.
- (45) Diaconescu, P. L.; Cummins, C. C. *J. Am. Chem. Soc.* **2002**, *124*, 7660–7661.
- (46) Jantunen, K. C.; Burns, C. J.; Castro-Rodriguez, I.; Da Re, R. E.; Golden, J. T.; Morris, D. E.; Scott, B. L.; Taw, F. L.; Kiplinger, J. L. *Organometallics* **2004**, *23*, 4682–4692.
- (47) Schelter, E. J.; Veauthier, J. M.; Thompson, J. D.; Scott, B. L.; John, K. D.; Morris, D. E.; Kiplinger, J. L. *J. Am. Chem. Soc.* **2006**, *128*, 2198–2199.
- (48) Silva, M.; Antunes, M. A.; Dias, M.; Domingos, A.; dos Santos, I. C.; Marcalo, J.; Marques, N. *Dalton Trans.* **2005**, 3353–3358.
- (49) Edelstein, N. M.; Lander, G. H. *Magnetic Properties*. In *The Chemistry of the Actinide and Transactinide Elements*, 3rd ed.; Morss, L. R., Edelstein, N. M., Fuger, J., Eds.; Springer: The Netherlands, 2006; Vol. 4, pp 2241–2247.
- (50) Arnold, P. L.; Patel, D.; Wilson, C.; Love, J. B. *Nature* **2008**, *415*, 315–318.
- (51) Miyake, C.; Hirose, M.; Ohya-Nishiguchi, H. *Inorg. Chim. Acta* **1989**, *165*, 179–183.
- (52) Selbin, J.; Ahmad, N.; Pribble, M. J. *J. Chem. Soc., Chem. Commun.* **1969**, 759–760.
- (53) Selbin, J.; Ahmad, N.; Pribble, M. J. *J. Inorg. Nucl. Chem.* **1970**, *32*, 3249–3258.
- (54) No resonances were observed in the ¹H NMR spectrum of **14** over the temperature range 0–100 °C.

Table 2. ^1H NMR Chemical Shift of the C_5Me_5 Protons in the $(\text{C}_5\text{Me}_5)_2\text{U}(=\text{N}-2,6\text{-}^i\text{Pr}_2\text{-C}_6\text{H}_3)(\text{X}/\text{Y})$ Complexes at 25 °C in C_6D_6

compound	δ (ppm)	$\Delta\nu_{1/2}$ (Hz)	compound	δ (ppm)	$\Delta\nu_{1/2}$ (Hz)
7 (X = F)	3.94	109	12 (Y = SPh)	4.57	83
8 (X = Cl)	4.92	84	13 (Y = C≡CPh)	4.11	80
9 (X = Br)	5.31	72	15 (Y = OPh)	3.33	71
10 (X = I)	5.78	125	16 (Y = Me)	3.30	63
11 (Y = OTf)	5.98	104	17 (Y = Ph)	3.00	117
			18 (Y = N=CPh ₂)	1.41	52

for this phenomena have been debated,^{56–58} it has been proposed for the uranium systems that the trend tracks with the amount of π -donation from the X/Y ligand to the metal center.^{55a,c} In effect, the better the π -donor, the more electron-rich the uranium center, manifesting in a larger shielding and an upfield shift of the auxiliary protons. In this regard, the chemical shift of a set of analogous protons for structurally related uranium complexes tracks with the electron density at the metal center as a result of the change in coordination environment in the complex. Therefore, **11** (L = OTf), which has the most downfield shifted C_5Me_5 resonance at δ 5.98 ppm, has the most electron deficient uranium center, presumably arising from poor donation from the weakly coordinating OTf ligand. The C_5Me_5 shifts for the halide series vary systematically with the identity and overall donating capacity of the halide ligand: **10** (X = I, δ 5.78 ppm) \rightarrow **9** (X = Br, δ 5.31 ppm) \rightarrow **8** (X = Cl, δ 4.92 ppm) \rightarrow **7** (X = F, δ 3.94 ppm), indicating that fluoride is the strongest donor compared to the other halogens. The chemical shift for the C_5Me_5 protons in **12** (δ 4.57 ppm) intersects the halide series, indicating that the polarizable SPh group is a better donor than the larger halides, although fluoride is still a better π -donor.⁵⁹ The C_5Me_5 resonance for $(\text{C}_5\text{Me}_5)_2\text{U}(=\text{N}-2,6\text{-}^i\text{Pr}_2\text{-C}_6\text{H}_3)(\text{C}\equiv\text{CPh})$ (δ 4.11 ppm) is slightly less than that of **7**, which is not surprising given that while the C≡CPh fragment is a strong σ -donor, its ability to π -donate is negligible.⁶⁰ The C_5Me_5 resonance for $(\text{C}_5\text{Me}_5)_2\text{U}(=\text{N}-2,6\text{-}^i\text{Pr}_2\text{-C}_6\text{H}_3)(\text{OPh})$ (δ 3.33 ppm) is further upfield, and the U^{V} -imido ketimide complex **18** is shifted to the largest upfield position: δ 1.41 ppm. Paired with the

geometric parameters, this peak position implies that the ketimide ligand is strongly donating to the uranium center, consistent with previous studies that suggest that a bond order > 1 exists between the uranium and $\text{N}_{\text{ketimide}}$.^{4,61} Interestingly, both the Me (δ 3.30 ppm) and Ph (δ 3.00 ppm) ligands are also strongly σ -donating to the uranium center in this system, to an extent approximately equal to or slightly better than the alkoxide derivative. Overall, given the relative positions of the C_5Me_5 resonances for the U^{V} -imido complexes, the trend in increasing donating ability for the X/Y ligand is $\text{OTf} < \text{I} < \text{Br} < \text{Cl} < \text{SPh} < \text{C}\equiv\text{CPh} < \text{F} < \text{OPh} \sim \text{Me} < \text{Ph} \ll \text{N}=\text{CPh}_2$. This is in good agreement with the electrochemical data which suggest a similar trend in ease of oxidation across the series (vide infra).

Electrochemistry. Cyclic and square-wave voltammetric data have been collected for $(\text{C}_5\text{Me}_5)_2\text{U}(=\text{N}-2,6\text{-}^i\text{Pr}_2\text{-C}_6\text{H}_3)(\text{X}/\text{Y})$ complexes **7–16** and **18** in ~ 0.1 M $[\text{Bu}_4\text{N}][\text{fluoroarylborate}]/\text{tetrahydrofuran}$ solution ($[\text{fluoroarylborate}]^- = [\text{B}(\text{C}_6\text{F}_5)_4]^-$ or $[\text{B}(3,5\text{-}(\text{CF}_3)_2\text{-C}_6\text{H}_3)_4]^-$). The potential data are summarized in Table 3, and typical cyclic voltammograms are illustrated in Figure 3. Data for **7–10**³² and **13**³⁴ have been previously reported, but are included here for completeness. We were unable to obtain voltammetric data for **17** because of very rapid decomposition of this complex in the supporting electrolyte solution. While similar problems were overcome previously for the fluoride complex (**7**)³² using low-temperature voltammetry to stabilize that complex for data collection, no such efforts were made for **17**.

The voltammetric data for the new U^{V} -imido complexes (**11**, **12**, **14–16**, **18**) reported in this work are completely consistent with that reported previously for the halides (**7–10**) and the acetylide complex (**13**). In particular, all these systems exhibit two chemically reversible one-electron redox transformations; an oxidation wave attributable to the $\text{U}^{\text{VI}}/\text{U}^{\text{V}}$ process and a reduction wave attributable to the $\text{U}^{\text{V}}/\text{U}^{\text{IV}}$ process. As illustrated in Figure 3, the separations between the anodic and cathodic peaks for these waves deviate, in some cases substantially, from the nominal electrochemically reversible value of 60 mV indicating that the heterogeneous electron-transfer rates vary significantly across this series.⁶² This behavior was reported previously for the halide complexes.³² Of greater interest is the variability in the half-wave potentials for these metal-based redox transformations across this series reflecting the role of the ancillary ligand in perturbing the redox energetics in these systems (Table 3). This perturbation appears to derive from an interplay between purely electrostatic effects (e.g., for the triflate complex **11**) and more intrinsic σ - and π -bonding interactions that shift electron density at the metal center thereby impacting the redox energetics. The overall effect across the series is quite dramatic for a seemingly small structural

(55) This trend in chemical shift for like protons as a function of halide has been seen for other paramagnetic uranium systems: (a) $[(1,3\text{-R}_2\text{-C}_5\text{H}_3)_2\text{UX}]_2$ (R = SiMe₃, CMe₃; X = F, Cl, Br, I): Lukens, W. W., Jr.; Beshouri, S. M.; Stuart, A. L.; Andersen, R. A. *Organometallics* **1999**, *18*, 1247–1252. (b) $(\text{C}_5\text{Me}_5)_3\text{UX}$ (X = F, Cl, Br): Evans, W. J.; Nyce, G. W.; Johnston, M. A.; Ziller, J. W. *J. Am. Chem. Soc.* **2000**, *122*, 12019–12020. (c) $(1,3\text{-R}_2\text{-C}_5\text{H}_3)_2\text{UX}_2$ (R = SiMe₃, CMe₃; X = F, Cl, Br, I): Lukens, W. W., Jr.; Beshouri, S. M.; Blosch, L. L.; Stuart, A. L.; Andersen, R. A. *Organometallics* **1999**, *18*, 1235–1246. (d) The ^1H NMR behavior of the $(\text{C}_5\text{H}_5)_3\text{UX}$ system has also been extensively studied not only where X = halide, but also for other donor groups such as OR, NR₂, SR, PR₂, etc.: Fisher, R. D. *NMR-Spectroscopy of organo-f-element and pre-lanthanoid complexes. In Fundamental and Technological Aspects of Organo-f-Element Chemistry*; Marks, T. J., Fragala, I. L., Eds.; NATO ASI Series - Series C: Mathematical and Physical Sciences. D. Reidel Publishing Company: Dordrecht, 1985; Vol. 155, p 294.

(56) Dhingra, M. M.; Ganguli, P.; Mitra, S. *Chem. Phys. Lett.* **1974**, *25*, 579–581.

(57) Drago, R. S.; Wayland, B. B. *Inorg. Chem.* **1968**, *7*, 628–630.

(58) LaMar, G. N.; Fischer, R. H.; Horrocks, W. D., Jr. *Inorg. Chem.* **1967**, *6*, 1798–1803.

(59) Figgis, B. N.; Hitchman, M. A. *Ligand Field Theory and Its Applications*; Wiley-VCH: New York, 2000.

(60) Elschenbroich, C.; Salzer, A. *Organometallics. A Concise Introduction*; VCH: Weinheim, Germany, 1989.

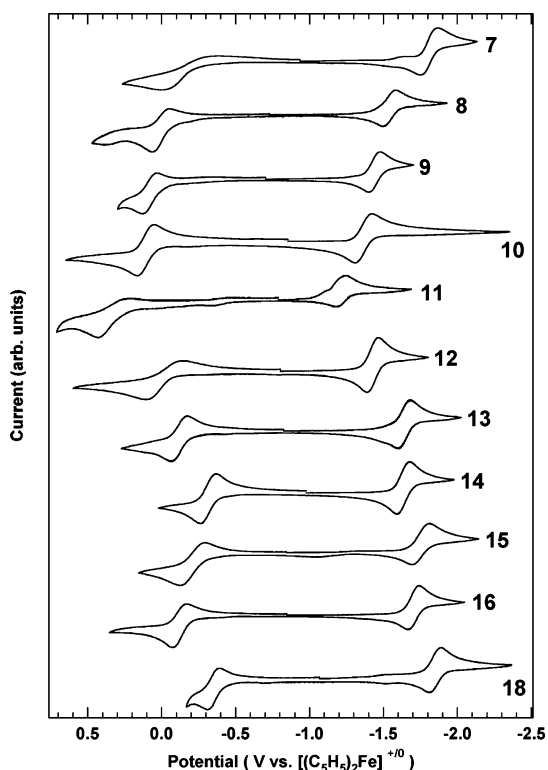
(61) Kiplinger, J. L.; Morris, D. E.; Scott, B. L.; Burns, C. J. *Organometallics* **2002**, *21*, 3073–3075.

(62) While positive-feedback IR compensation was employed in the collection of the voltammetric data, there is still some contribution from uncompensated solution resistance to the potential separation between cathodic and anodic peaks. Thus, deviations in the peak separation from 60 mV cannot be attributed solely to heterogeneous electron-transfer kinetic effects.

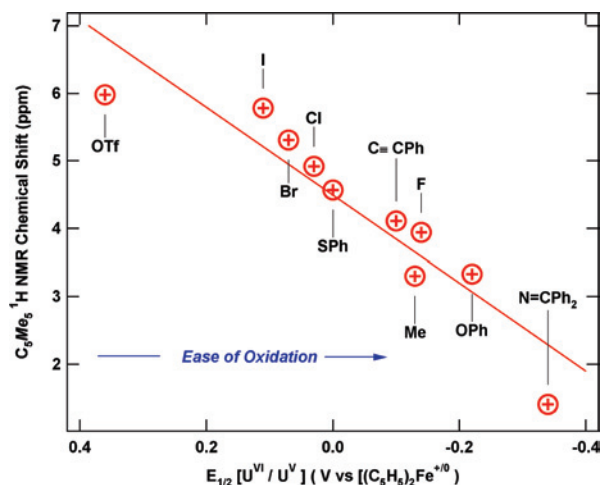
Table 3. Summary of Redox Potential Data^a for the (C₅Me₅)₂U(=N-2,6-ⁱPr₂-C₆H₃)(X/Y/L) Complexes **2**, **7–16** and **18** in ~0.1 M [Bu₄N][fluoroarylborate]^b/THF Solution at Room Temperature

U ^V complexes	X/Y	electrolyte anion ^b	$E_{1/2}(\text{U}^{\text{VI}}/\text{U}^{\text{V}})$ (V)	$E_{1/2}(\text{U}^{\text{V}}/\text{U}^{\text{IV}})$ (V)	$ \Delta E_{1/2} $ (V)	ref.
7 ^c	F	BAr _F	-0.14	-1.81	1.67	32
8	Cl	BAr _F	0.03	-1.52	1.55	32
9	Br	BAr _F	0.07	-1.44	1.51	32
10	I	B(C ₆ F ₅) ₄	0.11	-1.37	1.48	31, 32
11	OTf	BAr _F	0.36	-1.21	1.57	31, this work
12	SPh	BAr _F	0.00	-1.43	1.43	31, this work
13	C≡CPh	BAr _F	-0.10	-1.64	1.54	34
14	NPh ₂	BAr _F	-0.30	-1.65	1.35	this work
15	OPh	BAr _F	-0.22	-1.75	1.53	this work
16	Me	BAr _F	-0.13	-1.71	1.58	this work
18	N=CPh ₂	BAr _F	-0.34	-1.84	1.50	this work
					$ \Delta E_{1/2} _{\text{(ave)}}$	1.52 ± 0.03
U ^{IV} precursor	L	electrolyte anion ^b	$E_{1/2}(\text{U}^{\text{VI}}/\text{U}^{\text{IV}})$ (V)	$E_{1/2}(\text{U}^{\text{V}}/\text{U}^{\text{III}})$ (V)	$ \Delta E_{1/2} $ (V)	ref.
2	THF	BAr _F	-0.86	-2.40	1.54	28

^a All $E_{1/2}$ values are versus [(C₅H₅)₂Fe]⁺⁰ and were determined from the peak position in a square-wave voltammogram or from the average of the cathodic and anodic peaks in a cyclic voltammogram. ^b Electrolyte anion was either [B(3,5-(CF₃)₂-C₆H₃)₄]⁻ (BAr_F), or [B(C₆F₅)₄]⁻. ^c Although scan-rate dependent behavior was explored at ~-50 °C, potential calibration data were collected for this complex at room temperature using a freshly prepared solution.

**Figure 3.** Cyclic voltammograms for the (C₅Me₅)₂U(=N-2,6-ⁱPr₂-C₆H₃)(X/Y) complexes **7–16** and **18** in ~0.1M [Bu₄N][fluoroarylborate]/THF solution at 200 mV/s scan rate at a Pt electrode.

perturbation to the otherwise constant U^V-imido core (Table 1). If one considers the potential of the U^{VI}/U^V oxidation wave, the process shifts by ~0.7 V on going from the triflate complex (**11**) to the ketimide complex (**18**). As noted above, the chemical shift of C₅Me₅ ligand protons in the ¹H NMR spectra (Table 2) reflects the extent of electronic donation from the ancillary X/Y ligand to the metal center. Interestingly, there is an excellent linear correlation between these chemical shift values and the oxidation potentials (Figure 4), suggesting that there is a common origin, overall electron donation from the ancillary X/Y ligand to the metal, contributing to both observables.

**Figure 4.** Linear correlation between ¹H NMR chemical shift of the C₅Me₅ protons and oxidation potential for (C₅Me₅)₂U(=N-2,6-ⁱPr₂-C₆H₃)(X/Y). The correlation includes all ten available data points ($R^2 = 0.93$).

Finally, we note that the nearly constant potential separation between the U^{VI}/U^V and U^V/U^{IV} couples described previously³² is retained across this entire series of eleven complexes, with an average $|\Delta E_{1/2}|$ value of 1.52 ± 0.03 V. This implies that the factors responsible for (de)stabilizing the oxidation process are equally at play in shifting the reduction wave in the same direction. For example, the σ/π -donor ligands stabilize the U^{VI} oxidation state while concomitantly destabilizing the more electron-rich U^{IV} oxidation state by an approximately equal amount.

The existence of three different uranium oxidation states (U^{VI}, U^V, and U^{IV}) within this relatively narrow potential window is significant, and reminiscent of the behavior observed previously for (C₅Me₅)₂U^{IV}(ketimide)₂ complexes for which the U^V, U^{IV}, and U^{III} states all lie within an ~2.1 V range.^{4,63} This accessibility to three different oxidation states in these organouranium complexes having partial (ketimide) or full (imide) metal-ligand multiple bonding can be contrasted with the behavior seen for many other

(63) Morris, D. E.; Re, R. E. D.; Jantunen, K. C.; Castro-Rodriguez, I.; Kiplinger, J. L. *Organometallics* **2004**, *23*, 5142–5153.

(C₅Me₅)₂UL₂ complexes containing only simple σ -donor ligands (L) such as alkyl or halide. In this latter class of complexes only a single metal-based redox couple (e.g., U^{IV}/U^{III}) is observed under standard non-aqueous voltammetric conditions. The greater range of readily accessible oxidation states in the former systems is attributable to the stabilizing influence of the more covalent metal-ligand multiple bonding environment. Similar effects have been noted by Meyer and co-workers for Ru and Os polypyridyl complexes where the higher-valent metal centers are stabilized and hence become accessible through the formation of covalent metal oxo (M=O) bonds.⁶⁴

Electronic Spectroscopy. As noted previously,^{32,34} these pentavalent uranium complexes provide an excellent opportunity to explore in detail the electronic/molecular structure relationship. Their simple 5f¹ valence electronic configuration gives rise to relatively straightforward electronic spectra, and the essentially constant molecular structural framework provided by the (C₅Me₅)₂U(=N-2,6-*i*-Pr₂-C₆H₃) core enables a focus on perturbations introduced by the ancillary ligand (X/Y) in the metallocene wedge. Additionally, the imido ligand with its covalent multiple bonding to the metal center introduces additional molecular electronic states of both ligand-localized and charge-transfer character that have the potential to interact with the ligand-field (f-f) states in ways that provide additional diagnostics for the electronic structure and electronic interactions in these systems.

Consideration of the electronic spectra begins by examining the entire UV-visible-near IR region illustrated in Figure 5. For comparison purposes we have also included previously published spectra for complexes **7–10**³² and **13**.³⁴ There is remarkable consistency in the spectral band shapes and intensities, particularly for the spectra in the upper panel of Figure 5. The variability is somewhat greater in the spectra in the lower panel, although it should be noted that the intensity data for the methyl (**16**) and phenyl (**17**) complexes are less certain because these samples were prepared from material that was of an oily consistency that made accurate weighing problematic. The spectral assignments for the bands in the region from 10000–33000 cm⁻¹ have been described in detail previously and derive principally from transitions localized on the (C₅Me₅)₂U(=N-2,6-*i*-Pr₂-C₆H₃) core.³² Given the correlations among these spectra, it is likely that these assignments remain valid for all these complexes. Specifically, the lowest energy broad bands at ~10000 and 14000 cm⁻¹ are assigned to the two different spin components of the imido-to-metal charge-transfer transition: ⁴($\pi_{M=N} \rightarrow nb_{5f}$) and ²($\pi_{M=N} \rightarrow nb_{5f}$), respectively (nb = non-bonding). The higher energy bands in the UV-visible region are at least in part composed of $\pi_{M=N} \rightarrow \pi^*_{Ph}$ transitions. These assignments are all supported by density functional theory calculations.³² The strong spectral correlation across most of this series suggests that the ancillary (X/Y) ligand does not contribute significantly to electronic excited states within the region probed in our studies. The exceptions to this observation

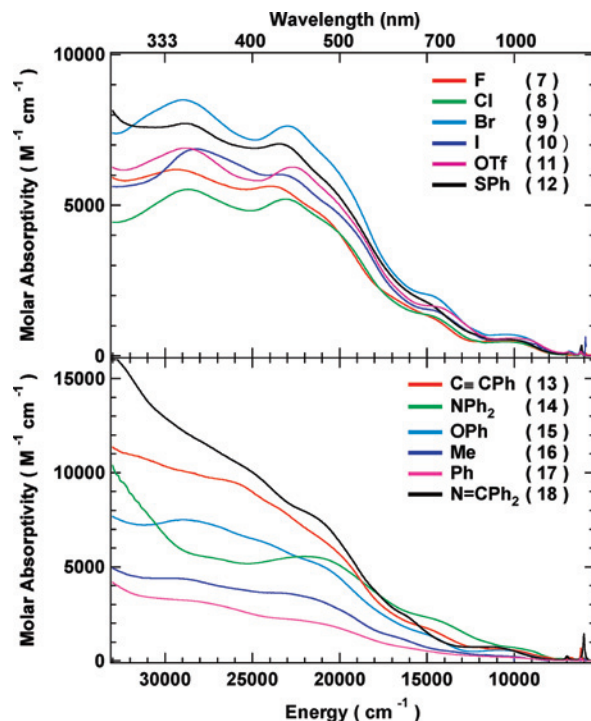


Figure 5. UV-visible-NIR electronic absorption spectra of the (C₅Me₅)₂U(=N-2,6-*i*-Pr₂-C₆H₃)(X/Y) complexes **7–18** in toluene solution at room temperature.

appear to be in the spectra for the acetylide (**13**) and ketimide (**18**) as evidenced by the substantially larger transition intensity in the higher energy region. Both of these ligands possess low-energy non-bonding, π and/or π^* orbitals that should contribute to the spectral density of states in this region.^{3,4,65,66} This becomes significant in the context of the f-f transition intensities discussed below.

The 5f¹ valence electronic configuration in all these complexes gives rise to a fairly simple f-orbital density of states. Spin-orbit coupling leads to only two manifolds of states: a ²F_{5/2} ground-state manifold and a ²F_{7/2} excited-state manifold. These manifolds will be further split according to the symmetry and strength of the crystal field imposed by the ligand environment. In the low symmetry of these U^V-imido complexes (nominally C_s symmetry), all orbital degeneracies should be removed leading to a total of seven states and six possible transitions. (Note that each state will still be a Kramer doublet as a consequence of the odd electron count.) Preliminary ligand-field calculations incorporating spin-orbit coupling reported by us previously³² for structurally simplified model surrogates of the fluoride (**7**) and iodide (**10**) complexes (i.e. (C₅Me₅)₂U(=N-C₆H₅)(X) (X = F, I)) are in general good agreement with published data and interpretations for 5f¹ systems in higher symmetry (e.g., *pseudo*-octahedral) environments such as the U^V hexahalides.²⁰ Specifically, the calculations predict that two transitions lie within ~2800 cm⁻¹ of the ground state and would not be observable in our experiments. The four

(65) Lichtenberger, D. L.; Renshaw, S. K.; Bullock, R. M. *J. Am. Chem. Soc.* **1993**, *115*, 3276–3285.

(66) Wong, C.-Y.; Che, C.-M.; Chan, M. C. W.; Han, J.; Leung, K.-H.; Phillips, D. L.; Wong, K.-Y.; Zhu, N. *J. Am. Chem. Soc.* **2005**, *127*, 13997–14007.

(64) Meyer, T. J.; Huynh, M. H. V. *Inorg. Chem.* **2003**, *42*, 8140–8160.

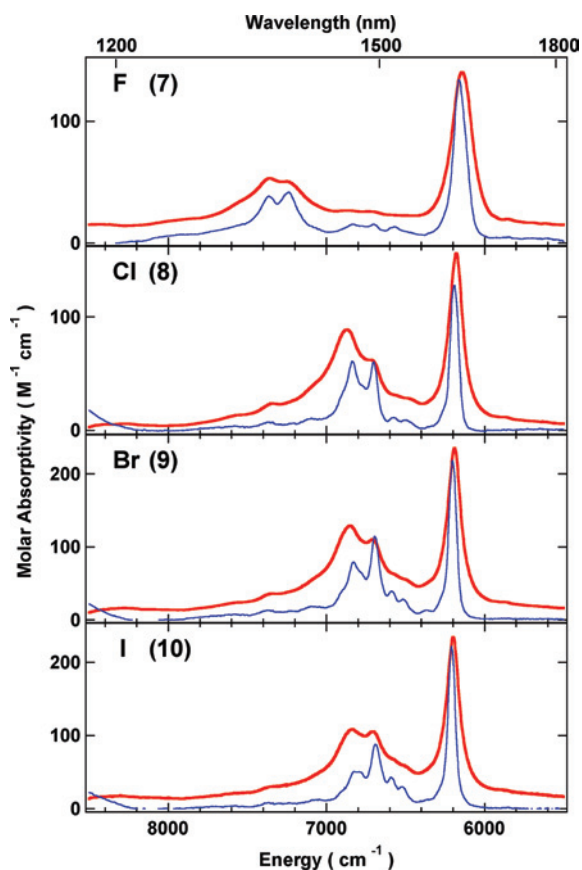


Figure 6. NIR electronic absorption spectra of the $(C_5Me_5)_2U(=N-2,6-{}^iPr_2-C_6H_3)(X)$ complexes **7–10** in toluene- d_8 solution at room temperature (red, offset for clarity) and 77 K (blue). Higher-energy tails from the visible spectra have been subtracted (see text).

remaining states are predicted to lie $6000–10000\text{ cm}^{-1}$ above the ground state, with the two lowest levels occurring at 6200 and 7100 cm^{-1} .

A set of narrow, lower intensity bands in this low energy spectral region is readily discernible in the data shown in Figure 5. These bands were isolated for better interpretation and comparison by fitting a Gaussian profile to the broad band at 10000 cm^{-1} and subtracting this broad band from the lower energy region. In addition, for several of the complexes, data were collected at 77 K in a toluene- d_8 glass to enhance the spectral resolution. Typical data for these f-f bands after this higher-energy background subtraction routine are illustrated in Figures 6 and 7. The spectra clearly are composed of many bands resulting from both pure electronic transitions and vibronic transitions built on the electronic transitions. At a qualitative level, the spectral data for all twelve complexes appear to be composed of two sets of bands. The first set occurs in the same energy range (with the most prominent band at $\sim 6000–6200\text{ cm}^{-1}$) for all complexes. The second set establishes greater distinction among the complexes. For the fluoride (**7**), diphenylamide (**14**), and phenoxide (**15**) the second set begins with the most prominent band at $\sim 7300\text{ cm}^{-1}$, whereas for all other complexes, this second set begins with the most prominent band occurring at lower energy ($\sim 6800–7000\text{ cm}^{-1}$). Note, however, that these ranges are in good agreement for all complexes with prediction from the ligand field/spin orbit

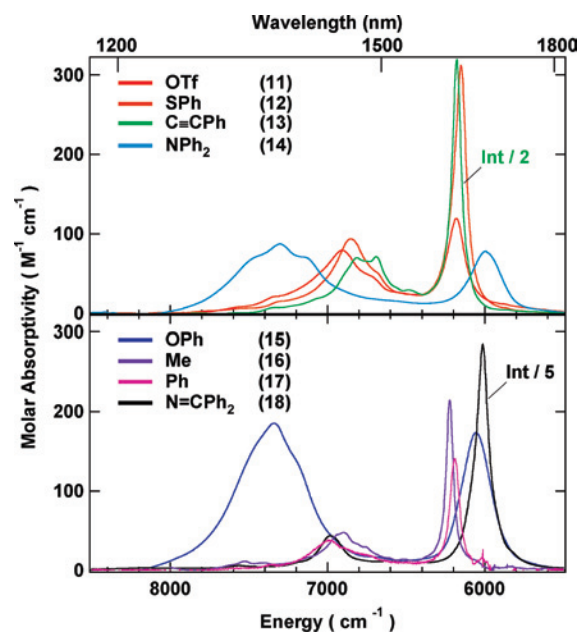


Figure 7. NIR electronic absorption spectra of the $(C_5Me_5)_2U(=N-2,6-{}^iPr_2-C_6H_3)(Y)$ complexes **11–18** in toluene- d_8 solution at room temperature. Higher-energy tails from the visible spectra have been subtracted (see text).

calculations performed previously for the fluoride and iodide model systems $(C_5Me_5)_2U(=N-C_6H_5)(X)$ ($X = F, I$).³²

Examination of the 77 K data (Figure 6) in this f-f spectral region for the four halide complexes provides some quantitative support for the interpretation that this region is comprised of *two* different sets of electronic transitions each of which has vibronic structure (instead of a single electronic transition with vibronic structure). First, there is a very weak feature in the room temperature data for each of the halide complexes at $\sim 5900\text{ cm}^{-1}$ that disappears in the 77 K spectra.³² This indicates that this feature is a vibronic hot-band, and therefore the most intense band in the $6100–6200\text{ cm}^{-1}$ region is an electronic origin. (Note that there is no inversion symmetry in these complexes, so dipole-selection rules associated with orbital parity are relaxed.) Next, the series of weak bands in the region just above this very intense feature ($\sim 6360, 6520,$ and 6590 cm^{-1}) is nearly identical for the chloride, bromide, and iodide complexes (with very minor shifts of all bands to slightly higher energy along the series $Cl < Br < I$) consistent with vibronic structure derived from vibrational modes of nearly identical energy for all three complexes. Since these features occur at nearly the same energy in all three spectra, they likely derive from modes localized on the $(C_5Me_5)_2U(=N-2,6-{}^iPr_2-C_6H_3)$ core, and do not involve the M–X interaction to an appreciable extent. The spectrum of the fluoride complex also has several weak vibronic features in this same region, as expected since it, too, has this same metallocene imido framework. To higher energy, however, there is a significant difference in the spectral data for the fluoride complex versus those of the other halides, with the next distinctive feature in the fluoride spectrum lying some $\sim 500\text{ cm}^{-1}$ to higher energy than those in the spectra of the other halides ($\sim 7250\text{ cm}^{-1}$ vs $\sim 6700\text{ cm}^{-1}$). This strongly suggests that this next series of bands derives from a new electronic transition (and related vibronic sidebands

to higher energy) that lies to higher energy in the fluoride complex than in the other halides because of the greater perturbative influence of the fluoride ion compared to that of the other halides on the metal-based energy levels.

The rich vibronic structure seen at 77 K for the halide complexes is less readily discernible in the room temperature data for the other non-halide systems (Figure 7), but the gross spectral features clearly fall into one of two categories; those with the higher energy set of f-f bands in the same higher-energy range as those of the fluoride complex (i.e., the diphenylamide (**14**) and the phenoxide (**15**)) and those whose spectra are more like those of the heavier halides. The crystal structure data (Table 1) that span most of the twelve complexes under consideration demonstrate that all complexes have very similar structural parameters, with the only significant difference being the identity of the ancillary ligand (X/Y) in the metallocene wedge, and the metal-ligand bond distance for this ligand. It is also expected that the spin-orbit coupling constant for U^V should remain essentially constant across the entire series of complexes. Thus, the spectral data provide an important opportunity to focus specifically on the contribution of the ancillary ligand to the splitting of the f-f states in these systems. In principal, these data can be used to arrange the ancillary ligands according to a spectrochemical or nephelauxetic series.^{67–69} However, the low symmetry of these complexes necessitates more parameters to describe the energy level splitting than can be deduced from the energies of just the two states identified in our data. We are pursuing additional density functional theory based calculations to enable a more quantitative assessment. It is clear that the complexes can be divided into two distinct classes based on these spectral data, and the grouping of the fluoride, diphenylamide, and phenoxide systems into the same class as suggested above is most consistent with the propensity of these ligands to interact strongly with the metal center through both σ - and π -donation that would be expected to lead to greater splitting of the $5f^1$ levels. However, the observation of slightly different categorizations of complexes based on these electronic spectral data versus the trend discussed above based on 1H NMR and redox potential data suggests that the splitting pattern for the f-f states reflects more subtle influences than simple σ/π electron-donation effects from the ancillary (X/Y) ligands.

The final consideration regarding these f-f spectral data concerns the intensities in the absorption bands. In classical coordination compounds of pentavalent uranium in *pseudo*-octahedral symmetry, such as the hexahalides, typical molar absorptivities are in the range $\sim 5\text{--}20\text{ M}^{-1}\text{ cm}^{-1}$.²⁰ In contrast, for the U^V -imido complexes herein, the molar absorptivities in the principal bands are in the range from ~ 100 to $\sim 1500\text{ M}^{-1}\text{ cm}^{-1}$. Clearly some of this discrepancy can be attributed to the fact that there is a relaxation in the electric dipole selection rules for these f-f transitions as the

symmetry is reduced from *pseudo*-octahedral in the hexahalides to $\sim C_s$ symmetry in the imido complexes. This effect alone likely cannot account for the observed more than 20-fold difference in intensities. It is more likely that the f-f transitions in the imido complexes gain intensity by coupling to the higher lying charge-transfer states that give rise to the spectral band shown in Figure 5. Such coupling should scale according to the transition intensity in these higher lying states and their energetic proximity to the f-f transitions.⁶⁷ This same mechanism was proposed previously to account for the unusually large f-f transition intensities in the near-IR spectra of $(C_5Me_5)_2U(\text{ketimide})_2$ complexes.^{4,63} In effect, some of the charge-transfer excited state character is mixed into the metal-localized f-f states inducing greater electric dipole-allowed character to the f-f transitions. The mixing is facilitated because there is common 5f orbital parentage in the states. Since the charge-transfer excited states have been shown to involve the $U=N$ imido bond, the observation of f-f intensity enhancement implicates f-orbital participation in the $U=N$ covalent bond. Hence, the intensity enhancement by this mixing of charge-transfer character is diagnostic of 5f orbital involvement in the bonding. In support of this proposed enhancement mechanism, we note in particular that the two complexes possessing the most intense f-f bands, the acetylide (**13**) and the ketimide (**18**), are also the complexes exhibiting the greatest intensities in the UV-visible transitions (Figure 5).

Conclusions

Given the increasing prominence that U^V complexes are gaining in the bonding and reactivity in actinide chemistry, the synthetic protocols reported herein provide a valuable entry into the synthesis of a variety of pentavalent uranium organometallic complexes $(C_5Me_5)_2U(=N-2,6\text{-}iPr_2-C_6H_3)(X/Y)$ (where $X = F, Cl, Br, I$; $Y = OTf, SPh, NPh_2, OPh, Me, Ph, C\equiv CPh, N=CPh_2$), which include the first examples of pentavalent uranium complexes with anionic sp , sp^2 , and sp^3 carbon moieties other than carbocyclic (C_5R_5 , C_7H_7 , C_8H_8) ligands. This is a strong complement to other reported routes to U^V organometallic species, and we have demonstrated that a multitude of substitution patterns can be achieved utilizing an array of reaction pathways—direct oxidation of the U^{IV} -imido precursor, salt metathesis, protonolysis, or insertion. That a wide range of substituents can be supported within the wedge of these U^V -imido complexes refutes prior assertions that pentavalent organouranium complexes are inherently unstable. The methods reported herein also avoid the use of silver and thallium salts (RCRA-listed), thereby greatly diminishing the generation of mixed radioactive hazardous waste and potential exposure to highly toxic thallium reagents.

The series of $(C_5Me_5)_2U(=N-2,6\text{-}iPr_2-C_6H_3)(X/Y)$ complexes with electronically diverse X/Y ligands was examined using a combination of structural analysis, magnetic susceptibility measurements, electrochemistry, and spectroscopy, which provides a coherent description of the electronic and magnetic structure of these pentavalent systems. The electrochemical analysis shows that the ligand framework can

(67) Lever, A. B. P. *Inorganic Electronic Spectroscopy*, 2nd ed.; Elsevier: Amsterdam, The Netherlands, 1984.

(68) Jorgensen, C. K. *Chem. Phys. Lett.* **1982**, *89*, 455–458.

(69) Krupa, J. C. *J. Solid State Chem.* **2005**, *178*, 483–488.

stabilize both the U^{IV} and U^{VI} oxidation states. An excellent linear correlation was observed between the chemical shift values of C₅Me₅ ligand protons in the ¹H NMR spectra and the oxidation potentials of the (C₅Me₅)₂U(=N-2,6-*i*-Pr₂-C₆H₃)(X/Y) compounds, suggesting that there is a common origin, overall σ - and π -donation from the ancillary X/Y ligand to the metal, contributing to both observables. Combined, these data allow for the following assessment of the overall donating ability of the X/Y ligand to the U^V metal center: OTf < I < Br < Cl < SPh < C≡CPh < F < [OPh ~ Me ~ Ph] ≪ NPh₂ < N=CPh₂.

With the spin-orbit coupling constant for U^V remaining essentially constant across the entire series of complexes, the absorption spectroscopic data provided an important opportunity to focus on the contribution of the X/Y ancillary ligand to the splitting of the f-f states in these systems. Interestingly, the complexes can be divided into two distinct classes based on the absorption spectroscopic data, with one group including X/Y = OTf, I, Br, Cl, SPh, C≡CPh, Me, Ph, and N=CPh₂, which are strong σ -donors and weaker π -donors in comparison to the other group containing the X/Y = F, NPh₂, and OPh, which interact strongly with the U^V metal center by both σ - and π -donation and lead to a larger splitting of the 5f¹ levels versus the former group of X/Y ligands.

When considered in the broader context of bonding in actinide chemistry, the (C₅Me₅)₂U(=N-2,6-*i*-Pr₂-C₆H₃)(X/Y) complexes also show distinct hallmarks of covalent metal-imide bonding interactions that are modulated to varying degrees by the X/Y ancillary ligand. The signatures of covalency include stabilization of multiple metal oxidation states [U^{IV}, U^V, and U^{VI}] and enhanced intensities in the intraconfiguration (f-f) transitions, such as the more than 20-fold enhancement in the f-f intensities observed for Y = C≡CPh and N=CPh₂, which are diagnostic indicators of covalency in the metal-ligand bonding interactions sustained by the acetylide and ketimide ligands in these pentavalent systems.

Experimental Section

General Considerations. Reactions and manipulations were performed in either a recirculating Vacuum Atmospheres NEXUS model inert atmosphere (N₂) drybox equipped with a 40CFM Dual Purifier NI-Train or using standard Schlenk techniques. Glassware was dried overnight at 150 °C before use. All NMR spectra were obtained in C₆D₆ using a Bruker Avance 300 MHz spectrometer. Chemical shifts for ¹H NMR spectra were referenced to solvent impurities. Melting points were determined with a Melt-Temp II capillary melting point apparatus equipped with a Fluke 50S K/J thermocouple using capillary tubes flame-sealed under nitrogen; values are uncorrected. Mass spectrometric (MS) analyses were obtained at the University of California, Berkeley Mass Spectrometry Facility, using a VG ProSpec (EI) mass spectrometer. Elemental analyses were performed at the University of California, Berkeley Microanalytical Facility, on a Perkin-Elmer Series II 2400 CHNS analyzer. X-ray data were collected using either a Bruker APEX2

or Bruker P4/CCD diffractometer. Structural solution and refinement was achieved using the SHELXL97 program suite.⁷⁰ Details regarding data collection are provided in the CIF files.

Celite (Aldrich), alumina (Brockman I, Aldrich), and 4 Å molecular sieves (Aldrich) were dried under dynamic vacuum at 250 °C for 48 h prior to use. All solvents (Aldrich) were purchased anhydrous, dried over KH for 24 h, passed through a column of activated alumina, and stored over activated 4 Å molecular sieves prior to use. (C₅Me₅)₂U(=N-2,4,6-*t*-Bu₃-C₆H₂) (**1**),³³ (C₅Me₅)₂U(=N-2,6-*i*-Pr₂-C₆H₃)(THF) (**2**),²⁵ Me₂Mg and Ph₂Mg(THF)₂,^{71,72} [Bu₄N][B(C₆F₅)₄]⁷³ and [Bu₄N][B(3,5-(CF₃)₂-C₆H₃)₄]⁷³ were prepared according to literature methods, and **11** and **12** were prepared as previously reported.³¹ KOPh and KNPh₂ were both prepared by refluxing a THF solution of HOPh and HNPh₂, respectively, over 1 equiv of KH for 24 h.⁷⁴

Caution! Depleted uranium (primary isotope ²³⁸U) is a weak α -emitter (4.197 MeV) with a half-life of 4.47 x 10⁹ years; manipulations and reactions should be carried out in monitored fume hoods or in an inert atmosphere drybox in a radiation laboratory equipped with α - and β -counting equipment.

Instrumentation and Sample Protocols. Electronic absorption spectral data were obtained for toluene or toluene-*d*₈ solutions of complexes over the wavelength range 300–2500 nm on a Perkin-Elmer Model Lambda 950 UV-visible-NIR spectrophotometer. Room temperature data were collected in 1 cm and 1 mm path length cuvettes loaded in the Vacuum Atmospheres drybox system described above run versus the appropriate toluene solvent reference. Samples were typically run at multiple dilutions to optimize absorbance in the UV-visible and near-infrared, respectively. Data collected at 77 K were obtained from samples in toluene-*d*₈ contained in medium-walled NMR tubes (503-PS from Wilmad/Lab Glass). The samples were immersed in an optical dewar with a quartz cold-finger (WG-850-Q-PTI) and run in a standard transmission spectrometer configuration versus air after ensuring the solutions glassed upon freezing. Pure toluene-*d*₈ was run under identical conditions to perform solvent corrections to the sample spectra post-data collection. No effort was made to be quantitative in determining extinction coefficients of the samples under these conditions. Spectral resolution was typically 2 nm in the visible region and 4–6 nm in the near-infrared in all cases.

Voltammetric data were obtained in the Vacuum Atmospheres drybox system described above. In addition, data for complex **7** were obtained in a Schlenk-line electrochemical cell immersed in a dry ice/2-propanol bath at ~–50 °C. All data were collected using a Perkin-Elmer Princeton Applied Research Corporation (PARC) Model 263 potentiostat under computer control with PARC Model 270 software. All sample solutions were ~1–2 mM in complex with 0.1 M [Bu₄N][B(3,5-(CF₃)₂-C₆H₃)₄] or [Bu₄N][B(C₆F₅)₄] supporting electrolyte in THF solvent.⁷³ All data were collected with the positive-feedback IR compensation feature of the software/

(70) (a) Bruker AXS, SAINT 7.06, Integration Software; Bruker Analytical X-ray Systems; Madison, WI, 2003. (b) Sheldrick, G. M. SADABS 2.03, Program for Adsorption Correction; University of Göttingen: Göttingen, Germany, 2001. (c) Sheldrick, G. M. SHELXTL 5.10, Structure Solution and Refinement Package; University of Göttingen: Göttingen, Germany, 1997.

(71) Tobia, D.; Baranski, J.; Rickborn, B. *J. Org. Chem.* **1989**, *54*, 4253–4256.

(72) Waggoner, K. M.; Power, P. P. *Organometallics* **1992**, *11*, 3209–3214.

(73) Barriere, F.; Geiger, W. E. *J. Am. Chem. Soc.* **2006**, *128*, 3980–3989.

(74) Barnhart, D. M.; Clark, D. L.; Grumbine, S. K.; Watkin, J. G. *Inorg. Chem.* **1995**, *34*, 1695–1699.

potentiostat activated to ensure minimal contribution to the voltammetric waves from uncompensated solution resistance (typically ~ 1 k Ω under the conditions employed). For experiments at ambient temperature, solutions were contained in PARC Model K0264 microcells consisting of a ~ 3 mm diameter Pt disk working electrode, a Pt wire counter electrode, and a Ag wire quasi-reference electrode. For the low temperature experiment, a Schlenk cell was employed consisting of Pt wire working and counter electrodes sandwiching a Ag wire quasi-reference electrode. Scan rates from 20–5000 mV/s were employed in the cyclic voltammetry scans to assess the chemical and electrochemical reversibility of the observed redox transformations. Half-wave potentials were determined from the peak values in the square-wave voltammograms or from the average of the cathodic and anodic peak potentials in the reversible cyclic voltammograms. Potential calibrations were performed at the end of each data collection cycle using the ferrocenium/ferrocene couple as an internal standard. Electronic absorption and cyclic voltammetric data were analyzed using Wavemetrics IGOR Pro (Version 4.0) software on a Macintosh platform.

Magnetic susceptibility data were collected using a Quantum Design Superconducting Quantum Interference Device (SQUID) magnetometer at 5 T from 2–350 K. The samples were sealed in a 5 mm Wilmad 505-PS NMR tube along with a small amount of quartz wool, which held the sample near the tube center. Contributions to the magnetization from quartz wool and the NMR tube were measured independently and subtracted from the total measured signal. Diamagnetic corrections were made with the use of Pascal's constants. Magnetic moments were determined from fits of the $1/\chi$ versus T data in the high temperature linear regimes.

Synthesis of $(C_5Me_5)_2U(=N-2,6-iPr_2-C_6H_3)(NPh_2)$ (14**).** A 125 mL side-arm flask equipped with a stir bar was charged with $(C_5Me_5)_2U(=N-iPr_2-C_6H_3)(I)$ (**10**) (0.25 g, 0.31 mmol), toluene (50 mL), $KNPh_2$ (0.077 g, 0.37 mmol) was added to the stirring dark brown solution, and the reaction was stirred at room temperature. After 12 h, the reaction mixture was filtered through a Celite-padded coarse frit and volatiles were removed from the filtrate. The residue was extracted into hexanes (50 mL) and filtered through a Celite-padded coarse porosity frit. The filtrate was collected, and the volatiles were removed under reduced pressure to give **14** as a brown solid (0.21 g, 0.25 mmol, 80%). X-ray quality samples of **14** were obtained by recrystallization from a toluene/hexamethyldisiloxane (1/1) mixture at -30 °C. Anal. Calcd for $C_{44}H_{57}N_2U$ (mol. wt. 851.97): C, 62.03; H, 6.74; N, 3.29. Found: C, 61.94; H, 6.37; N, 3.54. Mp = 205–207 °C. MS (EI, 70 eV): m/z 851 (M^+). $U^{VI/V} E_{1/2} = -0.30$ V, $U^{VI/IV} E_{1/2} = -1.65$ V (vs. $[(C_5H_5)_2Fe]^{+/0}$ in THF/0.1 M $[Bu_4N][B(3,5-(CF_3)_2-C_6H_3)_4]$). No resonances were observed in the 1H NMR of **14** over the temperature range 0–100 °C.

Synthesis of $(C_5Me_5)_2U(=N-2,6-iPr_2-C_6H_3)(OPh)$ (15**).** A 150 mL thick-walled Schlenk tube equipped with Teflon valve and a stir bar was charged with $(C_5Me_5)_2U(=N-2,6-iPr_2-C_6H_3)(I)$ (**10**) (0.25 g, 0.31 mmol), a magnetic stir bar, and toluene (50 mL). To the dark brown solution was added KOPh (0.049 g, 0.37 mmol) as an off-white powder. The reaction vessel was sealed and removed from the drybox to a fumehood, where it was placed in a 75 °C oil bath. After 12 h, the reaction was removed from heat, cooled to room temperature, and brought back into the drybox. The reaction was filtered through a Celite-padded coarse frit, and the volatiles were removed from the filtrate. The crude product was extracted into hexanes (50 mL), filtered through a Celite-padded coarse frit, and the volatiles removed under reduced pressure to give **15** as a brown solid (0.18 g, 0.23 mmol, 75%). X-ray quality samples of **15** were obtained by recrystallization from a concentrated hexam-

ethyldisiloxane solution at -30 °C. 1H NMR (C_6D_6 , 298 K): δ 49.91 (b, 1H, $CH(Me)_2$), 22.79 (1H, Ar-*H*), 16.43 (1H, Ar-*H*), 13.56 (1H, OPh), 11.43 (6H, $CH(Me)_2$), 10.21 (2H, OPh), 8.54 (1H, OPh), 3.33 (30H, $(C_5Me_5)_2$), -6.19 (6H, $CH(Me)_2$), -6.79 (1H, OPh), -11.33 (1H, Ar-*H*), -20.09 (b, 1H, $CH(Me)_2$). Anal. Calcd for $C_{38}H_{52}NOU$ (mol. wt. 776.85): C, 58.75; H, 6.75; N, 1.80. Found: C, 58.74; H, 6.96; N, 2.04. Mp = 197–199 °C. MS (EI, 70 eV): m/z 776 (M^+). $U^{VI/V} E_{1/2} = -0.22$ V, $U^{VI/IV} E_{1/2} = -1.75$ V (vs. $[(C_5H_5)_2Fe]^{+/0}$ in THF/0.1 M $[Bu_4N][B(3,5-(CF_3)_2-C_6H_3)_4]$).

Synthesis of $(C_5Me_5)_2U(=N-2,6-iPr_2-C_6H_3)(Me)$ (16**).** A 125 mL side-arm flask equipped with a stir bar was charged with $(C_5Me_5)_2U(=N-iPr_2-C_6H_3)(I)$ (**10**) (0.50 g, 0.62 mmol) and toluene (50 mL). Me_2Mg (0.045 g, 0.84 mmol) was added to the stirring dark brown solution followed by 1,4-dioxane (~ 0.5 mL), and the reaction was stirred at room temperature. After 12 h, the reaction mixture was filtered through a Celite-padded coarse frit, and volatiles were removed from the filtrate. The residue was extracted into hexanes (50 mL) and filtered through a Celite-padded coarse porosity frit. The filtrate was collected, and the volatiles were removed under reduced pressure to give **16** as a brown solid (0.30 g, 0.43 mmol, 70%) suitable for further reaction. 1H NMR (C_6D_6 , 298 K): δ 68.20 (b, 1H, $CH(Me)_2$), 28.57 (1H, Ar-*H*), 19.67 (1H, Ar-*H*), 15.20 (6H, $CH(Me)_2$), 3.30 (30H, $(C_5Me_5)_2$), -2.20 (3H, U-*Me*), -7.30 (6H, $CH(Me)_2$), -7.84 (1H, Ar-*H*), -16.06 (b, 1H, $CH(Me)_2$). Anal. Calcd for $C_{33}H_{50}NU$ (mol. wt. 698.79): C, 56.72; H, 7.21; N, 2.00. Found: C, 54.64; H, 7.07; N, 1.87. Despite numerous attempts, the long-term room temperature instability of complex **16** precluded obtaining good elemental analyses. $U^{VI/V} E_{1/2} = -0.13$ V, $U^{VI/IV} E_{1/2} = -1.71$ V (vs. $[(C_5H_5)_2Fe]^{+/0}$ in THF/0.1 M $[Bu_4N][B(3,5-(CF_3)_2-C_6H_3)_4]$).

Synthesis of $(C_5Me_5)_2U(=N-2,6-iPr_2-C_6H_3)(Ph)$ (17**).** A 125 mL side-arm flask equipped with a stir bar was charged with $(C_5Me_5)_2U(=N-iPr_2-C_6H_3)(I)$ (**10**) (0.50 g, 0.62 mmol), toluene (50 mL). $Ph_2Mg(THF)_2$ (0.40 g, 1.24 mmol) was added to the stirring dark brown solution followed by 1,4-dioxane (~ 0.5 mL), and the reaction was stirred at room temperature. After 12 h, the reaction mixture was filtered through a Celite-padded coarse frit, and volatiles were removed from the filtrate. The residue was extracted into hexanes (50 mL) and filtered through a Celite-padded coarse porosity frit. The filtrate was collected, and the volatiles were removed under reduced pressure to give **17** as a brown solid (0.38 g, 0.50 mmol, 80%) suitable for further reactions. 1H NMR (C_6D_6 , 298 K): δ 1H NMR (C_6D_6 , 298 K): δ 52.71 (b, 1H, $CH(Me)_2$), 30.79 (1H, Ar-*H*), 24.15 (1H, Ar-*H*), 14.65 (2H, Ar-*H*), 13.98 (6H, $CH(Me)_2$), 8.03 (3H, Ar-*H*), 3.00 (30H, $(C_5Me_5)_2$), -3.57 (6H, $CH(Me)_2$), -4.72 (1H, Ar-*H*), -15.47 (b, 1H, $CH(Me)_2$). The room temperature instability of **17** precluded elemental analysis.

Synthesis of $(C_5Me_5)_2U(=N-2,6-iPr_2-C_6H_3)(N=CPh_2)$ (18**).** **Method A - Protonolysis.** A 125 mL side-arm flask equipped with a stir bar was charged with $(C_5Me_5)_2U(=N-iPr_2-C_6H_3)(I)$ (**10**) (0.25 g, 0.31 mmol), toluene (50 mL). Me_2Mg (0.023 g, 0.42 mmol) was added followed by 1,4-dioxane (~ 0.25 mL), and the reaction was stirred for 12 h at room temperature. The resulting dark brown solution was filtered through a Celite-padded coarse frit. The filtrate was transferred to a 150 mL thick-walled Schlenk tube equipped with Teflon valve and a stir bar followed by benzophenone imine (0.067 g, 0.37 mmol) as a solution in toluene (5 mL). The reaction vessel was sealed and removed from the drybox to a fumehood, where it was placed in a 75 °C oil bath. After 12 h, the reaction was removed from heat, cooled to room temperature, and brought back into the drybox. The reaction was filtered through a Celite-padded coarse frit, and the volatiles were removed from the filtrate. The crude product was extracted into hexanes (50 mL), filtered

through a Celite-padded coarse frit, and volatiles were removed under reduced pressure to give **18** as a brown solid (0.023 g, 0.27 mmol, 86%).

Method B - Nitrile Insertion. A 125 mL side-arm flask equipped with a stir bar was charged with $(C_5Me_5)_2U(=N-^iPr_2-C_6H_3)(I)$ (**10**) (0.25 g, 0.31 mmol) and toluene (50 mL). $Ph_2Mg(THF)_2$ (0.20 g, 0.62 mmol) was added followed by 1,4-dioxane (~0.25 mL), and the reaction was stirred for 12 h at room temperature. The resulting dark brown solution was filtered through a Celite-padded coarse frit. Benzonitrile (0.038 g, 0.37 mmol) was added to the dark brown filtrate as a solution in toluene (5 mL), and the resulting reaction was stirred at room temperature. After 12 h, the reaction was filtered through a Celite-padded coarse frit and the volatiles were removed from the filtrate. The crude product was extracted into hexanes (50 mL), filtered through a Celite-padded coarse frit, and volatiles were removed under reduced pressure to give **18** as a brown solid (0.025 g, 0.28 mmol, 91%).

X-ray quality samples of **18** were obtained by recrystallization from a concentrated hexane solution at $-30\text{ }^\circ\text{C}$. $^1\text{H NMR}$ (C_6D_6 , 298 K): δ 46.50 (b, 1H, $CH(Me)_2$), 28.79 (1H, Ar-*H*), 23.81 (1H, Ar-*H*), 21.69 (1H, Ar-*H*), 11.40 (6H, $CH(Me)_2$), 9.61 (3H, Ar-*H*), 7.92 (4H, Ar-*H*), 1.58 (30H, $(C_5Me_5)_2$), -0.58 (2H, Ar-*H*), -2.38 (6H, $CH(Me)_2$), -8.17 (b, 1H, $CH(Me)_2$), -18.30 (1H, Ar-*H*). Anal. Calcd for $C_{45}H_{57}N_2U$ (mol. wt. 863.98): C, 62.56; H, 6.65; N, 3.24.

Found: C, 63.58; H, 6.39; N, 3.57. Mp = 216–218 $^\circ\text{C}$. MS (EI, 70 eV): m/z 863 (M^+). $U^{VI/V} E_{1/2} = -0.34\text{ V}$, $U^{VI/V} E_{1/2} = -1.84\text{ V}$ (vs $[(C_5H_5)_2Fe]^{+/0}$ in THF/0.1 M $[Bu_4N][B(3,5-(CF_3)_2-C_6H_3)_4]$).

Acknowledgment. For financial support of this work, we acknowledge LANL (Director's PD Fellowship to C.R.G. and E.J.S.; Frederick Reines PD Fellowship to E.J.S.), the LANL G. T. Seaborg Institute (PD Fellowships to C.R.G. and E.J.S.; summer graduate student fellowship to A.E.V.), the Division of Chemical Sciences, Office of Basic Energy Sciences, Heavy Element Chemistry program, and the LANL Laboratory Directed Research & Development program. This work was carried out under the auspices of the National Nuclear Security Administration of the US. Department of Energy at Los Alamos National Laboratory under Contract DE-AC5206NA25396.

Supporting Information Available: Magnetic susceptibility data for **11–15** and **18** and crystallographic data for **14** and **18** (PDF, CIF). This material is available free of charge via the Internet at <http://pubs.acs.org>.

IC8017375